J. Fluid Mech. (2024), *vol*. 999, A20, doi:10.1017/jfm.2024.981

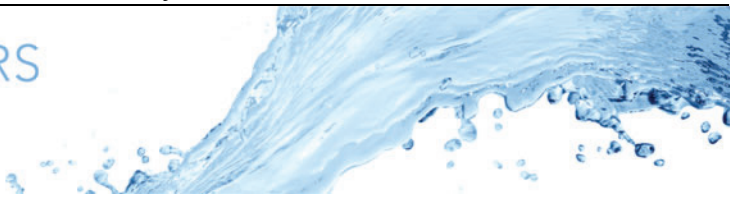

A Reynolds analogy model for compressible wall turbulence

Cheng Cheng[1,2] **and Lin Fu**[1,3,4,5,†]

[1]Department of Mechanical and Aerospace Engineering, The Hong Kong University of Science and Technology, Clear Water Bay, Kowloon, Hong Kong

[2]Institute for Advanced Study, The Hong Kong University of Science and Technology, Clear Water Bay, Kowloon, Hong Kong

[3]Department of Mathematics, The Hong Kong University of Science and Technology, Clear Water Bay, Kowloon, Hong Kong

[4]HKUST Shenzhen-Hong Kong Collaborative Innovation Research Institute, Futian, Shenzhen 518045, PR China

[5]Center for Ocean Research in Hong Kong and Macau (CORE), The Hong Kong University of Science and Technology, Clear Water Bay, Kowloon, Hong Kong

(Received 28 June 2024; revised 4 October 2024; accepted 5 October 2024)

In the present study, we propose a Reynolds analogy model for compressible wall turbulence. This model is demonstrated to be able to alleviate the defects of the generalized Reynolds analogy model (GRA) (Zhang *et al.*, *J. Fluid Mech.*, vol. 739, 2014, pp. 392–420), and maintains its success in describing the mean velocity–temperature relation. Furthermore, the present model is superior to the GRA in depicting the relationship between their fluctuating fields and also bridges the gap between the phenomenological model and the mathematical representation of the Reynolds analogy. The key points of the present model are validated by analysing the data of compressible wall-bounded turbulence with different Mach numbers, Reynolds numbers and wall thermal conditions.

Key words: compressible boundary layers, turbulent boundary layers, turbulence theory

1. Introduction

On the surfaces of high-speed flying vehicles, the generated compressible wall-bounded turbulence would bring about non-negligible heat transfer, which is as crucial as the

† Email address for correspondence: linfu@ust.hk

aerodynamic force for safe flight. To achieve a precise design of future high-speed aircraft, it is thus essential to accurately predict both the thermal and aerodynamic force effects in compressible wall turbulence. One research approach is to delineate the similarities between the temperature and velocity fields, and further seek the velocity–temperature relationship in compressible wall turbulence, which is generally called the Reynolds analogy. This type of research has undergone a long period of development and achieved a satisfactory answer in the past decade with the help of direct numerical simulations (DNS). The deduced relations have also been deployed for modelling purposes (Griffin, Fu & Moin 2023; Song, Zhang & Xia 2023; Chen, Gan & Fu 2024; Cheng & Fu 2024*a*; Cheng *et al.* 2024; Hasan *et al.* 2024). As early as the 1930s, Busemann (1931) and Crocco (1932) independently deduced the first velocity–temperature relation for laminar flows by assuming that the Prandtl number (Pr) of fluid is unity. This relation was then extended by van Driest (1951) for turbulent boundary layers. Within their frameworks, a very strong analogy between these two instantaneous fluctuating fields is made, which reads as

$$H' = U_w u', \tag{1.1}$$

where H and u denote the total enthalpy and the streamwise velocity, respectively, and ξ' represents the fluctuating component of a variable ξ, which is the difference between the instantaneous value of ξ and its Reynolds averaged statistic $\bar{\xi}$. Here U_w is a constant for a boundary layer. For the mean fields, the relation is

$$\bar{H} - \bar{H}_w = U_w \bar{u}, \tag{1.2}$$

where the subscript 'w' denotes the wall quantity. Regarding an adiabatic boundary layer, the exact relationship between the instantaneous u' and T' can be deduced from (1.1), i.e. $T' = -\bar{u}u'/C_p$, where C_p and T denote the specific heat at constant pressure and the temperature field, respectively. Based on this relation, Morkovin (1962) further proposed several derivative inferences, which are dubbed as the strong Reynolds analogy (SRA).

The assumption $Pr = 1$ in the Crocco–Busemann relation is too idealized, because for air, $Pr \approx 0.7$. This deviation results in differences between the DNS results and the SRA predictions in later studies. To circumvent this deficiency, Walz (1962) hypothesized that a mixed Prandtl number, $Pr_m = C_p(\bar{\mu} + \bar{\mu}_t)/(\bar{k} + \bar{k}_t)$, is a constant, where μ, μ_t, k and k_t denote the viscosity, the eddy viscosity, the thermal conductivity and the eddy thermal conductivity, respectively. Meanwhile, the mean temperature is considered to be only a function of $\bar{u}$, and thus the Walz equation is derived. Its equivalent form is

$$\bar{H}_r - \bar{H}_w = U_w \bar{u}, \tag{1.3}$$

where $\bar{H}_r = C_p[\bar{T} + r\bar{u}^2/(2C_p)]$ is called the local recover enthalpy, and r is the recovery factor. Compared with (1.2), (1.3) suggests that the local excess recovery enthalpy is in direct proportion to the magnitude of mean velocity field. Walz's equation improves the Crocco–Busemann relation and agrees with DNS well in adiabatic turbulent boundary layers (Pirozzoli, Grasso & Gatski 2004; Duan & Martin 2011; Fu *et al.* 2021). However, for diabatic flows, its performance is not that good (Duan & Martin 2011; Zhang, Duan & Choudhari 2018; Huang, Duan & Choudhari 2022).

For the relationship between the fluctuating fields, the most vital modification is the celebrated Huang's strong Reynolds analogy (HSRA) (Huang, Coleman & Bradshaw 1995), incorporating the phenomenological model of Gaviglio (1987), which takes the form of

$$Pr_t T'_{rms}/\partial_y \bar{T} = u'_{rms}/\partial_y \bar{u}, \tag{1.4}$$

where $Pr_t \equiv (\overline{\rho v' u'}/\overline{\rho v' T'})(\partial \bar{T}/\partial \bar{u})$ is the turbulent Prandtl number (ρ and v denote the fluid density and the wall-normal velocity, respectively) and the subscript 'rms' represents

the root mean square value (r.m.s.). This relation works well for wall turbulence with different wall thermal conditions (Pirozzoli *et al.* 2004; Duan & Martin 2011; Huang *et al.* 2022).

The first empirical relation of mean fields which performs well for distinct wall thermal conditions was proposed by Duan & Martin (2011). They introduced a non-dimensional recovery enthalpy, which is defined as $\bar{H}_r^* = (\bar{H}_r - \bar{H}_w)/(\bar{H}_{r\delta} - \bar{H}_w)$, and found that $\bar{H}_r^*$ is a unique function of $\bar{u}/\bar{u}_\delta$ for all DNS data, where the subscript 'δ' refers to the quantities evaluated at the boundary edge. When calorically perfect gas is assumed, a new velocity–temperature relation can be obtained.

Thereafter, the most systematic model is the generalized Reynolds analogy theory (GRA) proposed by Zhang *et al.* (2014). They generalized the velocity–enthalpy relation by introducing a general recovery enthalpy H_g,

$$\bar{H}_g - \bar{H}_w = U_w \bar{u}, \tag{1.5}$$

where $H_g = C_p T + r_g u^2/2$, and r_g is an extended form of r. Simultaneously, a residual temperature ϕ' is also introduced to build a loose analogy between the fluctuating velocity and temperature fields, namely,

$$H_g' + C_p \phi' = U_w u'. \tag{1.6}$$

Multiplying (1.6) by $(\rho v)'$ and averaging, r_g can be solved as

$$r_g = \frac{C_p}{\bar{u}} \left[\left. \frac{\partial \bar{T}}{\partial \bar{u}} \right|_w - \frac{1}{\overline{Pr_e}} \frac{\partial \bar{T}}{\partial \bar{u}} \right], \tag{1.7}$$

where $\overline{Pr_e}$ is called the effective Prandtl number by Zhang *et al.* (2014), whose definition is

$$\overline{Pr_e} \equiv \frac{\overline{Pr_t}}{1+\varepsilon}, \quad \overline{Pr_t} \equiv \frac{\overline{(\rho v)' u'}}{\overline{(\rho v)' T'}} \frac{\partial \bar{T}}{\partial \bar{u}}, \quad \varepsilon \equiv \frac{\overline{(\rho v)' \phi'}}{\overline{(\rho v)' T'}}. \tag{1.8a–c}$$

Herein $\overline{Pr_t}$ is a new definition of the turbulent Prandtl number, and its value is only a little different from that of Pr_t in the outer layer of a boundary layer at a high Mach number (Zhang *et al.* 2014). Substitution of (1.7) into (1.5) yields a differential equation for the mean fields,

$$\bar{T} - \frac{\bar{u}}{2} \left[\left. \frac{\partial \bar{T}}{\partial \bar{u}} \right|_w + \frac{1}{\overline{Pr_e}} \frac{\partial \bar{T}}{\partial \bar{u}} \right] = \bar{T}_w. \tag{1.9}$$

Simultaneously, for the fluctuating fields, their relation can be also deduced by substituting (1.7) into (1.6):

$$T' + \phi' = \frac{1}{\overline{Pr_e}} \frac{\partial \bar{T}}{\partial \bar{u}} u'. \tag{1.10}$$

Zhang *et al.* (2014) further adopted the simplest model for $\overline{Pr_e}$ and assumed $\overline{Pr_e} = 1$, and thus (1.9) becomes solvable. The deduced mean velocity–temperature relation is

$$\frac{\bar{T}}{\bar{T}_\delta} = \frac{\bar{T}_w}{\bar{T}_\delta} + \frac{\bar{T}_{rg} - \bar{T}_w}{\bar{T}_\delta} \frac{\bar{u}}{\bar{u}_\delta} + \frac{\bar{T}_\delta - \bar{T}_{rg}}{\bar{T}_\delta} \left(\frac{\bar{u}}{\bar{u}_\delta} \right)^2, \tag{1.11}$$

where $\bar{T}_{rg} = \bar{T}_\delta + r_g \bar{u}_\delta^2/(2C_p)$. Interestingly, through introducing the well-known Reynolds analogy factor and treating it as a constant, (1.11) can recover the empirical

relation of Duan & Martin (2011). For the fluctuating fields, Zhang *et al.* (2014) modelled ϕ' as $(\overline{(\rho v)'\phi'}/\overline{(\rho v)'u'})u'$, and the HSRA can be restored with Pr_t in (1.4) replaced by $\overline{Pr_t}$. Hereafter, we name this modified form as MHSRA.

Although the deductions of the GRA are successful in depicting the $\bar{u}$–$\bar{T}$ relation, we want to remember some points that are not clearly clarified in previous work. Firstly, the GRA is an overdetermined system. For a given flow, the unknown functions are r_g and ϕ'. However, there are three related equations, i.e. (1.5), (1.6) and the assumption $\overline{Pr_e} = 1$. Secondly, the physical meaning of ϕ' is not clearly identified. The core assumptions of the GRA are the existence of the residual temperature ϕ' and the constant value of $\overline{Pr_e}$. The latter is also associated with the existence of ϕ', because the extra wall-normal heat flux transfer originating from ϕ' in the definition of $\overline{Pr_e}$ (i.e. ε) acts as an effective correction to $\overline{Pr_t}$, making up its systematic deviation from unity. So we may ask two questions. What is the physical significance of ϕ'? Is it a physically real field that exists independently of T', or is it just a component of T'? Thirdly, if $-\phi'$ is a component of T', (1.10) implies that the whole velocity fluctuating field shares a duality relation with just a portion of the temperature fluctuating field. This scenario is kind of counterintuitive.

Motivated by these confusions, we try to propose a new Reynolds analogy theory. We find that this model might provide a good solution to each issue, and shed light on some subtle details of the u–T coupling. Meanwhile, the newly introduced residual quantities (temperature and velocity) in our model are of clear physical significance, which bridge the gap between the phenomenological model and the mathematical representation of the Reynolds analogy.

2. A Reynolds analogy model

We begin with the key point proposed by Zhang *et al.* (2014), that it is the local recovery enthalpy, rather than the total enthalpy, that remains constant in the shear region for air flow over an adiabatic wall. Also, we also adopt r_g to account for the effects of $Pr \neq 1$ in flows over diabatic walls. However, we hypothesize that it is not u, but a new velocity u_e, named the local effective velocity, which constitutes the local effective recovery enthalpy (H_e), i.e. $H_e = C_pT + r_g u_e^2/2$. The local effective velocity can be decomposed into two components,

$$u_e = u + \chi', \tag{2.1}$$

where χ' can also be regarded as a residual velocity with zero mean value but non-negligible fluctuation, and thus $\bar{u}_e = \bar{u}$. On the other hand, the generalized mean enthalpy–velocity relation is

$$\bar{H}_e - \bar{H}_w = U_w \bar{u}_e, \tag{2.2}$$

and U_w can be determined to be $U_w = (C_p \partial \bar{T}/\partial \bar{u}_e)_w$. Equation (2.2) can be expanded as

$$C_p\bar{T} + \tfrac{1}{2} r_g \overline{u^2} + \tfrac{1}{2} r_g \overline{\chi'^2} + r_g \overline{u'\chi'} - C_p\bar{T}_w = U_w\bar{u}. \tag{2.3}$$

For the relationship between the fluctuating local effective enthalpy and velocity, the following formula can be introduced:

$$H_e' + C_p\phi' = U_w u_e', \tag{2.4}$$

where $H_e' = C_pT' + r_g\bar{u}_e u_e'$. In our model, the residual temperature ϕ' is still included to describe the temperature fields of flows over adiabatic walls. Following Zhang *et al.* (2014),

r_g can be solved after multiplying (2.4) by $(\rho v)'$ and averaging, that is,

$$r_g = \frac{C_p}{\bar{u}_e}\left[\frac{U_w}{C_p} - \frac{\overline{(\rho v)'(T'+\phi')}}{\overline{(\rho v)'(u'+\chi')}}\right]. \tag{2.5}$$

Gaviglio (1987) observed that, for a compressible boundary layer, the intensities of the velocity and temperature fluctuations carried by large-scale eddies are in direct proportion to the gradients of their mean quantities, respectively. And their corresponding ratios are positively related to the velocity length scale and the temperature length scale, respectively. In our model, we treat $T'+\phi'$ and $u'+\chi'$ as the pure temperature and velocity fluctuations that are directly determined by the mean fields, and thus, carried by the large-scale eddies (see more detailed analyses in § 3). In this regard, combining our propositions and the phenomenological model of Gaviglio (1987), we can directly link the ratio of the wall-normal momentum and heat flux transfers in the right-hand side of (2.5) with the gradients of the mean fields,

$$\frac{\overline{(\rho v)'(T'+\phi')}}{\overline{(\rho v)'(u'+\chi')}} = \alpha\frac{\partial \bar{T}}{\partial \bar{u}}, \tag{2.6}$$

where α is a constant. Hence, (2.5) can further be deduced as

$$r_g = \frac{C_p}{\bar{u}}\left[\left.\frac{\partial \bar{T}}{\partial \bar{u}}\right|_w - \alpha\frac{\partial \bar{T}}{\partial \bar{u}}\right], \tag{2.7}$$

where the relation $\bar{u}_e = \bar{u}$ is used. The differential equation for the mean temperature can be obtained by substituting (2.7) into (2.3) and using $\overline{u^2} \approx \bar{u}^2$, which reads as

$$\bar{T} - \frac{\bar{u}}{2}\left[\left.\frac{\partial \bar{T}}{\partial \bar{u}}\right|_w + \alpha\frac{\partial \bar{T}}{\partial \bar{u}}\right] + \frac{r_g\left(\overline{\chi'^2} + 2\overline{u'\chi'}\right)}{2C_p} = \bar{T}_w, \tag{2.8}$$

and the u'–T' relation can be derived by substituting (2.7) into (2.4), namely,

$$T' + \phi' = \alpha\frac{\partial \bar{T}}{\partial \bar{u}}\left(u' + \chi'\right). \tag{2.9}$$

It can be seen that if we take α to be $1/\overline{Pr}_e(=1)$ and ignore the effect of χ', the present model can restore to the GRA. It is particularly noteworthy that the present model is well-posed, because the number of the unknown functions (χ', r_g and ϕ') is the same as that of the relevant equations ((2.2), (2.4) and (2.6)) for a given flow (α is not an unknown quantity, see the related discussion in § 4). Furthermore, following the procedures outlined in Zhang *et al.* (2014), it can be mathematically proved that the similarity between the Reynolds averaged momentum and energy equations permits the solution expressed by (2.2) and (2.4).

As the temperature fluctuation can be recognized as a passive scalar even in compressible wall turbulence (Cheng & Fu 2024*b*), we can consider the u–T coupling through the lens of a control system. The fluctuating velocity and temperature fields can be treated as the input and output, respectively, whereas the related transfer function is determined by the mean profiles of these two fields. The fluctuating temperature field is essentially the response of the temperature field to the velocity field. If this response is perfect, their coherence, which can be appraised by their correlated function, would be

tight. Under these circumstances, the duality relation between u' and T' is well-established. In the parlance of this view, within the framework of the SRA, the magnitude of the transfer function is $|\bar{u}/C_p|$. However, the relation is built in an instantaneous sense, and thus the SRA is generally poorly agreed with the real flows. For the HSRA, the corresponding transfer function is $|(1/Pr_t)(\partial\bar{T}/\partial\bar{u})|$, which is only valid for the r.m.s. values of T' and u'. For the MHSRA, the counterpart is $|(1/\overline{Pr_t})(\partial\bar{T}/\partial\bar{u})|$, if ϕ' is modelled as $(\overline{(\rho v)'\phi'}/\overline{(\rho v)'u'})u'$. As can be seen, the duality relation between u' and T' is partially broken in the GRA due to the inclusion of ϕ'.

However, the present model suggests that the input–output relation cannot be completely built between u' and T' without considering the influences of ϕ' and χ'. In other words, the duality relation between u' and T' is more seriously broken in our model than in the GRA. Besides, the differential equation (2.8) cannot be explicitly solved, as the statistical characteristic of the term $r_g(\overline{\chi'^2} + 2\overline{u'\chi'})/2C_p$ is unknown. In the next section, we will analyse the physical significance of χ', and assess its role in determining the distributions of mean fields.

3. Physical significance of χ' and ϕ'

Up to now, it is natural to ask two questions. What is the physical significance of χ' and ϕ'? Are they introduced as temporary variables to alleviate the theoretical crisis of the SRA, or are they physically meaningful quantities with genuine physical implications? We conjecture that the answers are hidden in the physical meanings of (2.6) and (2.9). These two equations suggest that $T' + \phi'$ and $u' + \chi'$ are the pure temperature and velocity fluctuations that are directly controlled by the mean fields, and carried by the large-scale eddies. That is to say, $-\phi'$ and $-\chi'$ are the components of T' and u' that are not manipulated by the mean gradients. Because the mean shear is typically believed to be the energy source of the large-scale motions in shear flows (Jiménez 2018), it implies that $-\phi'$ and $-\chi'$ must be two small-scale quantities which keep away from the influences of the mean gradients and are not directly related to the surrounding energy-containing motions. These analyses are reminiscent of the work of Cheng & Fu (2023), who reported that the u–T coupling in compressible wall turbulence is sustained by energy-containing motions, just as the description of the phenomenological model proposed by Gaviglio (1987). It can be seen that, compared with the GRA, the current model better captures the dominance of the large-scale eddies described phenomenologically by Gaviglio (1987), with the mean fields as the connecting factors. Therefore, within the current framework, the assumption (2.6) is natural and reasonable.

Next, we combine the DNS data of compressible wall turbulence with a mature mathematical tool to verify our propositions. The DNS database of channel flows used in the present study for detailed analysis is built in our previous study (Cheng & Fu 2022). These cases are performed in a computational domain of $4\pi h \times 2\pi h \times 2h$ in the streamwise (x), spanwise (z) and wall-normal (y) directions, respectively. Herein, h denotes the channel half-height. Three cases at bulk Mach numbers (M_b) 0.8, 1.5 and 3.0 are selected, and their bulk Reynolds numbers (Re_b) are 17 000, 20 020 and 15 000, respectively. They are of the highest friction Reynolds numbers in our dataset at the corresponding M_b, and denoted as Ma08Re17K, Ma15Re20K and Ma30Re15K, respectively. The details of each simulation and its validation are provided at length in Cheng & Fu (2022). We will not repeat them here for the sake of brevity.

The diagnostic tool deployed in the present study is the spectral linear stochastic estimation (SLSE). The SLSE is a data-driven tool for investigating the multiphysics

couplings in both incompressible and compressible wall-bounded turbulence. It is capable of measuring the degree of the linear coherence between two variables in the flow field, and estimating the instantaneous signal of a target physical quantity with another quantity as input. Note that the estimated signal is linearly coherent with the input signal, due to the linear nature of the SLSE. In the present study, we first resort to the SLSE to extract the component of T' that bears a linear coherence with the streamwise velocity fluctuation u' at a given wall-normal position y in turbulent channel flows. It takes the form of

$$T'_l(y) = F_{x,z}^{-1}\left\{H_{Tu}(\lambda_x, \lambda_z; y)\, F_{x,z}\left[u'(y)\right]\right\}, \tag{3.1}$$

where T'_l is the component of T' sharing a linear coherence with u' at the wall-normal position y. In this regard, the uncorrelated component can be calculated as $T'_{nl} = T' - T'_l$. In the expression, $F_{x,z}$ and $F_{x,z}^{-1}$ denote the two-dimensional (2-D) fast Fourier transform and the inverse 2-D fast Fourier transform in the streamwise and the spanwise directions, respectively. Here H_{Tu} is the transfer kernel, which gauges the correlation between $\widehat{T'}(y)$ and $\widehat{u'}(y)$ at streamwise length scale λ_x and spanwise length scale λ_z, and can be calculated as

$$H_{Tu}(\lambda_x, \lambda_z; y) = \frac{\left\langle \widehat{T'}(\lambda_x, \lambda_z; y)\, \overset{\times}{\widehat{u'}}(\lambda_x, \lambda_z; y)\right\rangle}{\left\langle \widehat{u'}(\lambda_x, \lambda_z; y)\, \overset{\times}{\widehat{u'}}(\lambda_x, \lambda_z; y)\right\rangle}, \tag{3.2}$$

where $\langle\cdot\rangle$ denotes the ensemble averaging, $\widehat{u'}$ and $\widehat{T'}$ are the Fourier coefficients of u' and T', respectively, and $\overset{\times}{\widehat{u'}}$ represents the complex conjugate of $\widehat{u'}$. Similarly, we can also extract the component of u' that holds a linear relationship with T', that is,

$$u'_l(y) = F_{x,z}^{-1}\left\{H_{uT}(\lambda_x, \lambda_z; y)\, F_{x,z}\left[T'(y)\right]\right\}, \tag{3.3}$$

where the kernel function H_{uT} can be constructed by analogy. The uncorrelated component can be calculated as $u'_{nl} = u' - u'_l$. On the other hand, we also can measure the overall response intensity by comparing the r.m.s. values of T' and u', namely, T'_{rms}/u'_{rms}. The ratios between T'_l and u', and T'_l and u'_l, can be defined by analogy. They can be compared with the following response functions, i.e.

$$f_1(y) = \left|\frac{1}{Pr_t}\frac{\partial \bar{T}}{\partial \bar{u}}\right|, \quad f_2(y) = \left|\frac{\partial \bar{T}}{\partial \bar{u}}\right|. \tag{3.4a,b}$$

Note that, the Pr_t in $f_1(y)$ is computed from the DNS data, and we observe that the difference between the values of Pr_t and $\overline{Pr_t}$ is negligible for the DNS data of channel flows considered in the present study, hence we will not make a distinction between the HSRA and the MHSRA. Specifically, $f_1(y)$ is the transfer function suggested by the HSRA (MHSRA) and $f_2(y)$ is the transfer function indicated by the GRA and the present model. If the HSRA (MHSRA) is true, the distribution of $f_1(y)$ should match well with that of T'_{rms}/u'_{rms} for each case (see (1.4)). If the present model is established, the distribution of $f_2(y)$ should agree with that of $T'_{l,rms}/u'_{l,rms}$ (see (2.9)), whereas for the establishment of the GRA, the profile of $f_2(y)$ should be in close agreement with that of $T'_{l,rms}/u'_{rms}$ (see (1.10)). Additionally, to facilitate comparison, three ratio functions are defined as $r_1 = (|(1/Pr_t)(\partial \bar{T}/\partial \bar{u})|u'_{rms})/T'_{rms}$, $r_2 = (|(\partial \bar{T}/\partial \bar{u})|u'_{l,rms})/T'_{l,rms}$ and $r_3 = (|(\partial \bar{T}/\partial \bar{u})|u'_{rms})/T'_{l,rms}$, which are the quantitative metrics corresponding to the HSRA, the present model, and the GRA.

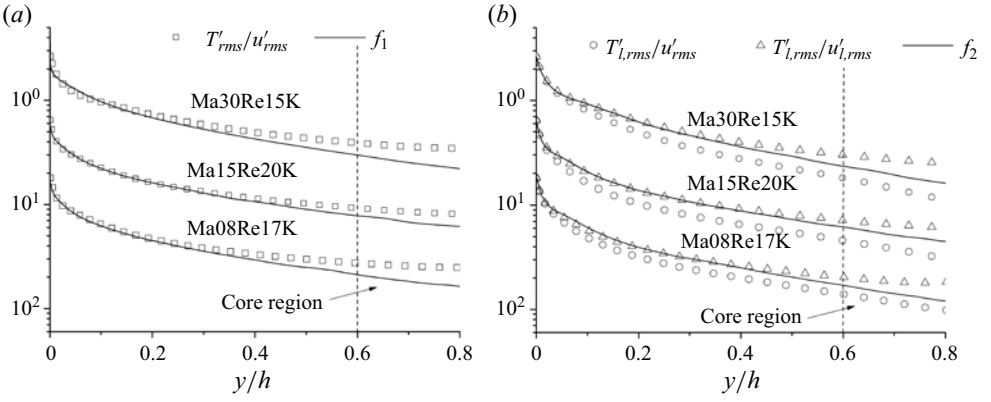

Figure 1. Variations of (*a*) T'_{rms}/u'_{rms} and (*b*) $T'_{l,rms}/u'_{rms}$ and $T'_{l,rms}/u'_{l,rms}$ for all cases of channel flows. The response functions given by different Reynolds analogy models are represented by solid lines in each panel: $f_1(y)$ is the transfer function suggested by the HSRA (MHSRA) and $f_2(y)$ is the transfer function indicated by the GRA and the present model.

Figure 1(*a*) shows the variations of T'_{rms}/u'_{rms} for all cases of channel flows mentioned above, and the distributions of f_1 are added for comparison. It can be found that the magnitudes of T'_{rms}/u'_{rms} agree tolerably well with those of f_1 within $0 < y/h < 0.6$, below the core region of a channel. This observation is consistent with the finding of Huang *et al.* (1995) for compressible channel flows. It suggests that the overall response of T' follows the prediction of the HSRA, as well as the MHSRA.

In figure 1(*b*), we concentrate on the components of T' and u' that are linearly coherent with each other, namely, T'_l and u'_l. One can notice that the distributions of f_2 are consistent with those of $T'_{l,rms}/u'_{l,rms}$ for $0 < y/h < 0.6$, at least within the Mach numbers under consideration. The accuracy is rather similar to that of the HSRA (MHSRA) (see the variations of r_1, r_2 and r_3 for each case shown in figure 2). This is an interesting finding, because it implies that it is essentially T'_l, rather than T', that would response to u'_l, rather than u', if the transfer function is f_2; that is to say,

$$T' - T'_{nl} = \frac{\partial \bar{T}}{\partial \bar{u}}(u' - u'_{nl}). \tag{3.5}$$

It is noted that (3.5) may be not fully accurate in an instantaneous sense, but it suggests the key input–output relation between them, and is valid in a statistical sense. Compared with (2.9), the establishment of (3.5) underscores the fact that

$$-\phi' = T'_{nl}, \quad -\chi' = u'_{nl}. \tag{3.6a,b}$$

That is to say, $-\phi'$ and $-\chi'$ are not physically real fields that exist independently of T' and u', respectively, but just the components of T' and u' that are not linearly correlated with u' and T', respectively. Furthermore, this result also suggests $\alpha = 1$. Interestingly, it is precisely the assumed value of $\overline{Pr_e}$. More discussion regarding the value of α is given in § 4. On the other hand, if the input–output relation follows (1.10) predicted by the GRA, it is u', rather than u'_l, that would be linearly coherent with the T'_l, and the response intensity should be f_2. Figure 1(*b*) also shows the variations of $T'_{l,rms}/u'_{rms}$ for comparison. Obviously, it deviates from the prediction of the GRA (f_2) for each case. It suggests the existence of χ', and thus demonstrating the superiority of the present model in depicting the u'–T' relation and providing direct evidence of the phenomenological model proposed

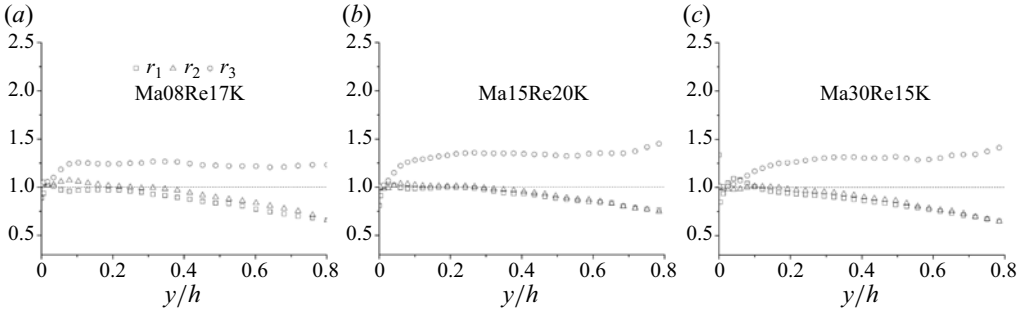

Figure 2. Variations of $r_1 = (|(1/Pr_t)(\partial\bar{T}/\partial\bar{u})|u'_{rms})/T'_{rms}$, $r_2 = (|(\partial\bar{T}/\partial\bar{u})|u'_{l,rms})/T'_{l,rms}$ and $r_3 = (|(\partial\bar{T}/\partial\bar{u})|u'_{rms})/T'_{l,rms}$ for three channel flows at different M_b.

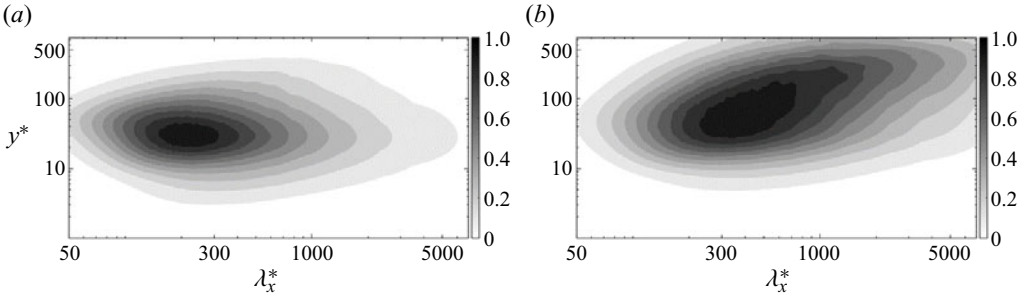

Figure 3. (*a*) Premultiplied streamwise spectrum of T'_{nl}; (*b*) premultiplied streamwise spectrum of u'_{nl}. The case Ma15Re20K is taken into consideration. Each spectrum is normalized by its maximum value, and the streamwise wavelength is scaled by the semilocal units at $y^* \approx 20$.

by Gaviglio (1987). Moreover, Guarini *et al.* (2000) pointed out that the $u' - T'$ relation (2.4) implies the $\bar{u}$–$\bar{T}$ relation (2.2). In this regard, the improvement of the present model over the GRA is fundamental.

Another fact supports our judgement is that for a compressible wall boundary layer with a cold wall, the fluctuating velocity and temperature fields show a strong decorrelation in the proximity of the wall-normal region where $\partial\bar{T}/\partial\bar{y} \approx 0$, (see figure 14*a* of Cogo *et al.* (2023)). According to (3.5) and (3.6*a*,*b*), near the extreme point of a mean temperature profile where $\partial\bar{T}/\partial\bar{y} \approx 0$, the right-hand side of (3.5) should be zero. In this way, we can deduce that $T'_l \approx 0$ and $\phi' = -T'_{nl} \approx -(T' - T'_l) \approx -T'$. As can be seen, ϕ' happens to be $-T'$ that decorrelates with u', i.e. the component of T' that is not linearly correlated with u'. Moreover, figure 3 shows the premultiplied streamwise spectra of T'_{nl} and u'_{nl} for the case Ma15Re20K with the streamwise wavelength scaled by the semilocal units at $y^* \approx 20$. One can notice that their spectral peaks are located at $\lambda_x^* \approx 250$ and $\lambda_x^* \approx 400$, respectively. Here, we use the superscript '$*$' to represent the normalization in semilocal units. It can be seen that their streamwise length scales are shorter than those of the temperature and velocity streaks populating the near-wall region ($\lambda_x^* \approx 1000$) (Cheng & Fu 2022). This observation is consistent with the analyses conducted above, which assert that $-\phi'$ and $-\chi'$ ought to be two small-scale quantities which are not directly related to the surrounding energy-containing motions controlled by the mean fields.

We also verify our model in supersonic and hypersonic turbulent boundary layers. The DNS database of compressible turbulent boundary layers used here is built by Zhang *et al.*

Case	M_∞	Re_∞	$T_\infty(K)$	T_w/T_r	T_w/T_e	$L_x \times L_y \times L_z$	Re_τ	$t_s u_\infty/\delta_i$
M20T050	2.0	9081	220	0.5	0.85	$24.8\delta_i \times 8.1\delta_i \times 8.7\delta_i$	665–806	589.4
M20T100	2.0	26631	220	1.0	1.68	$30.1\delta_i \times 8.2\delta_i \times 10.6\delta_i$	674–819	584.6
M80T050	8.0	422782	51.8	0.5	4.82	$13.8\delta_i \times 6.8\delta_i \times 5.0\delta_i$	650–715	271.5
M80T100	8.0	1186116	51.8	1.0	8.72	$14.3\delta_i \times 7.0\delta_i \times 5.1\delta_i$	601–654	231.1

Table 1. The parameters of compressible turbulent boundary layers. Here M_∞, Re_∞ and T_∞ are the freestream Mach number, Reynolds number and temperature, respectively; T_w/T_r denotes the ratio of isothermal wall temperature and recovery temperature; T_w/T_e denotes the ratio of isothermal wall temperature and boundary edge temperature; L_x, L_y and L_z are the lengths of selected domain in the streamwise, wall-normal and spanwise directions, respectively; δ_i and Re_τ are the inlet boundary layer thickness and the range of the friction Reynolds number of the selected domain, respectively; and $t_s u_\infty/\delta_i$ is the time period used to accumulate statistics.

(2022). For each case, a selected domain is adopted for analysing, and the parameters are provided in table 1. It can be observed that the Reynolds number effects are negligible because the corresponding variation of Re_τ is small. Under the circumstances, the 2-D SLSE introduced above can be deployed. More details about the computational set-ups and the numerical methods regarding the DNS of this dataset can be found in Zhang *et al.* (2022).

Figure 4(*a*,*c*,*e*,*g*) show the distributions of T'_{rms}/u'_{rms} and $f_1(y)$ within the boundary layers, and figure 4(*b*,*d*,*f*,*h*) display the variations of $T'_{l,rms}/u'_{rms}$, $T'_{l,rms}/u'_{l,rms}$ and $f_2(y)$ for all cases. It is noted that the Pr_t in the definition of $f_1(y)$ is replaced by $\overline{Pr_t}$ herein, as previous studies showed that this modified version of the turbulent Prandtl number is less sensitive to the freestream Mach number and wall temperature condition at the edge of the turbulent boundary layer (Zhang *et al.* 2014; Cogo *et al.* 2023). It can be observed that for all cases, the profiles of $f_1(y)$ agree roughly with those of T'_{rms}/u'_{rms}, irrespective of the Mach number and wall thermal condition. It implies the success of the MHSRA (HSRA), which is documented in numerous previous studies (Guarini *et al.* 2000; Duan & Martin 2011; Huang *et al.* 2022). However, significant deviations can still be traced within the intermittent layers ($y/\delta > 0.8$). Similar inconsistency can also be found in previous studies, for example, figure 9(*b*) of Zhang *et al.* (2018) and figure 18(*c*) of Cogo *et al.* (2023).

On the other hand, it is apparent that the distributions of $T'_{l,rms}/u'_{l,rms}$ match reasonably well with those of $f_2(y)$ in most regions of the boundary layers for all cases, even in the intermittent layers, see figure 4(*b*,*d*,*f*,*h*). Observable deviations can only be traced around the extreme points of the mean temperature profiles for the cases with cold walls. This is acceptable, because the gradient of the mean temperature is zero around this kind of point, which leads to the breakdown of the u'_l–T'_l relation (3.5). By contrast, for all cases, the distributions of $T'_{l,rms}/u'_{rms}$ are not in tune with those of $f_2(y)$ unequivocally. One can also refer to the distributions of r_1, r_2 and r_3 for all cases displayed in figure 5. Combining with the results of compressible channel flows reported above, we might claim that the present model is superior to the GRA in depicting the relationship between fluctuating fields of velocity and temperature in canonical compressible wall turbulence. Of course, it also needs more data for validation in the future.

Moreover, the present model seems to work better than the MHSRA (HSRA) in the intermittent layers of compressible boundary layers, irrespective of the Mach number and wall thermal condition, for the cases under consideration (see figures 4 and 5). By the way, in the core region of an internal flow, the acoustic component of the fluctuating

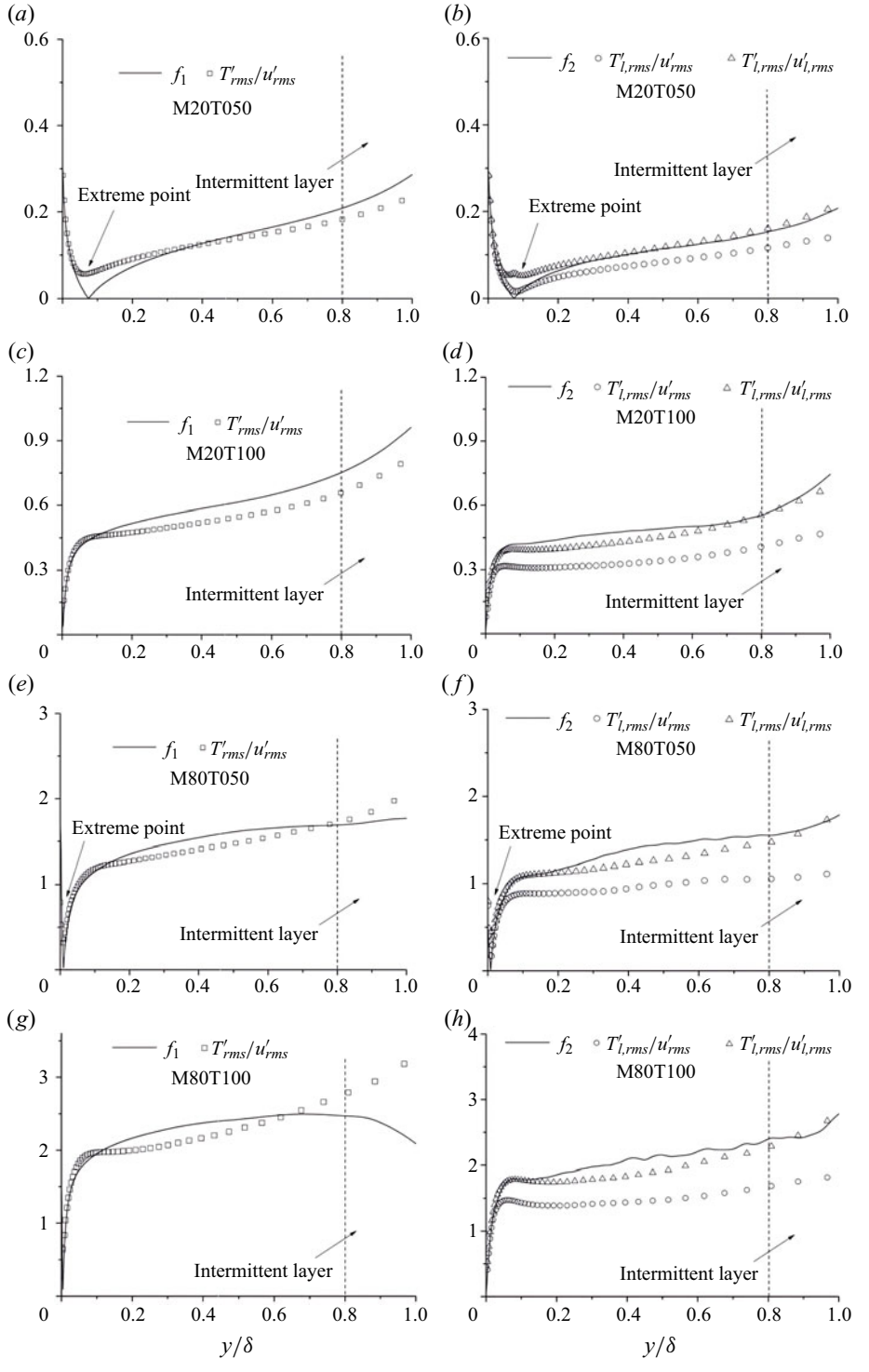

Figure 4. Variations of (a,c,e,g) T'_{rms}/u'_{rms} and (b,d,f,h) $T'_{l,rms}/u'_{rms}$ and $T'_{l,rms}/u'_{l,rms}$ for all the cases of turbulent boundary layers. The response functions given by different Reynolds analogy models are represented by solid lines in each panel: $f_1(y)$ is the transfer function suggested by the MHSRA (HSRA) and $f_2(y)$ is the transfer function indicated by the GRA and the present model. Here, δ is the mean boundary layer thickness of the selected domain for each case.

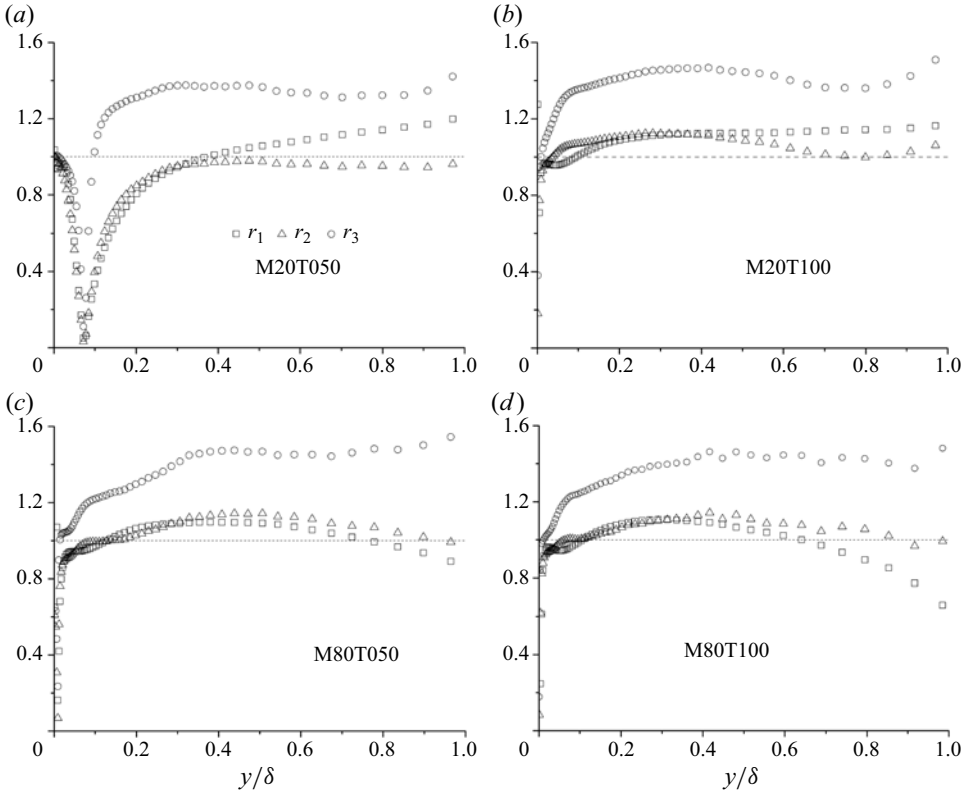

Figure 5. Variations of $r_1 = (|(1/\overline{Pr_t})(\partial\bar{T}/\partial\bar{u})|u'_{rms})/T'_{rms}$, $r_2 = (|(\partial\bar{T}/\partial\bar{u})|u'_{l,rms})/T'_{l,rms}$ and $r_3 = (|(\partial\bar{T}/\partial\bar{u})|u'_{rms})/T'_{l,rms}$ for compressible turbulent boundary layers with different wall thermal conditions and freestream Mach numbers.

motions is dominant (Zhang *et al.* 2014; Cheng & Fu 2024*b*), as a result, the basics of each Reynolds analogy model might not hold, leading to the significant deviations of the MHRSA (HSRA) and the present model illustrated in figure 1.

4. Implications for the $\bar{u}$–$\bar{T}$ relation

One may ask, why does the GRA fail to accurately characterize the relationship of the fluctuating fields, but is able to effectively capture the distributions of the mean fields in canonical flows? This is due to the negligible effect of the term $r_g(\overline{\chi'^2} + 2\overline{u'\chi'})/2C_p$ in (2.8) in determining the $\bar{u}$–$\bar{T}$ relation. According to (3.6*a*,*b*), this term can be rewritten as

$$\frac{r_g\left(\overline{\chi'^2} + 2\overline{u'\chi'}\right)}{2C_p} = \frac{r_g\left[\overline{u'^2_{nl}} - 2\overline{(u'_{nl} + u'_l)u'_{nl}}\right]}{2C_p} \approx -\frac{r_g\overline{u'^2_{nl}}}{2C_p}, \tag{4.1}$$

where the assumption $\overline{u'_l u'_{nl}} = 0$ is adopted. Here u'_{nl} is a small-scale fluctuating quantity, and the magnitude of $-r_g\overline{u'^2_{nl}}/2C_p$ is significantly smaller than those of other terms associated with mean fields in (2.8), and thus can be ignored. As a result, an analytic solution of (2.8) becomes available with $\alpha = 1$, that is (1.11). We note in passing that, ignoring this small-scale fluctuating term is equivalent to adopting the approximation

$\overline{u_e^2} \approx \bar{u}_e^2 = \bar{u}^2$, which is widely deployed for modelling the canonical wall turbulence (Zhang *et al.* 2014).

Finally, it is instructive to discuss the value of α. Ignoring the fluctuating term and solving (2.8) yields the general solution without additional assumptions,

$$\bar{T} = \bar{T}_w + A \left.\frac{\partial \bar{T}}{\partial \bar{u}}\right|_w \bar{u} + B\bar{u}^{2\alpha}, \tag{4.2}$$

where $A = \alpha/(2\alpha - 1)$ and B is a constant. Differentiating (4.2) with respect to $\bar{u}$ and taking the value on the wall boundary, one has $\alpha = 1$. It indicates that $\alpha = 1$ is a requirement for the mathematical self-consistency of the present model, which is fully consistent with the results shown in figures 1(*b*) and 4(*b*,*d*,*f*,*h*). As such, the well-established $\bar{u}$–$\bar{T}$ relation (1.11) proposed by Zhang *et al.* (2014) can also be deduced under the framework of the present model by replacing the artificial assumption $\overline{Pr_e} = 1$ with a stricter mathematical derivation of $\alpha = 1$. On the other hand, because the $\bar{u}$–$\bar{T}$ relation (1.11) has been broadly validated in numerous studies of compressible wall turbulence, including pipe flows (Zhang *et al.* 2014), channel flows (Modesti & Pirozzoli 2016) and turbulent boundary layers (Huang *et al.* 2022), it implies that $\alpha = 1$ should be generic. Unlike the arbitrary assumption of $\overline{Pr_e} = 1$ in the GRA, $\alpha = 1$ carries distinct physical significance as per (2.6). It suggests that the momentum and heat transfers, which are controlled by the gradients of the mean fields, are dynamically similar. This similarity is not sensitive to the Mach number and the geometry of the flows. In simpler terms, within the regime controlled by the mean fields, the input–output relation between u' and T' holds a certain universality.

5. Discussion and concluding remarks

As the u'–T' relations are shown to be related to the multiscale eddies in the boundary layers, it is of significance to examine their Reynolds number dependence. A new set of DNS data of supersonic channel flows is used. Three cases at $Re_b = 3000$, 9400 and 20 020 are selected, and their bulk Mach numbers are all 1.5. Validation of this dataset is also given in Cheng & Fu (2022). They are denoted as Ma15Re3K, Ma15Re9K and Ma15Re20K, respectively. Figure 6(*a*) shows the variations of r_1 for all three cases. Remarkable Reynolds number dependence can be traced. Within $0.3 < y/h < 0.7$, the magnitude of r_1 approaches unity as the increase of the Reynolds number. It suggests that the HSRA (MHSRA) will be more accurate at higher Reynolds numbers. Figure 6(*b*) shows the counterparts of r_2. Interestingly, clear Reynolds number dependence can also be observed, and the values of r_2 are closer to unity for high Reynolds numbers in the outer region.

In conclusion, in the present study, we are dedicated to proposing a Reynolds analogy model for compressible wall turbulence. This model is demonstrated to be able to alleviate the defects of the GRA, and maintains its success in describing the $\bar{u}$–$\bar{T}$ relation. Furthermore, the present model is superior to the GRA in depicting the u'–T' relation. The key points of the present model are validated by analysing the data of compressible wall-bounded turbulence with different Mach numbers, Reynolds numbers and wall thermal conditions.

The present study provides a new perspective of the velocity–temperature coupling in compressible wall turbulence, and may trigger new studies on this topic. For example, as the $u_l' - T_l'$ relation is universal for compressible wall turbulence, further work can

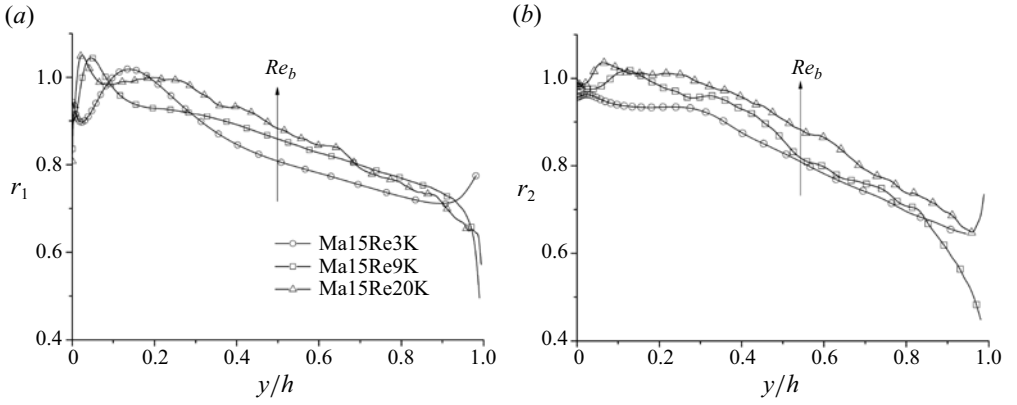

Figure 6. Variations of (*a*) $r_1 = (|(1/Pr_t)(\partial\bar{T}/\partial\bar{u})|u'_{rms})/T'_{rms}$, (*b*) $r_2 = (|\partial\bar{T}/\partial\bar{u}|u'_{l,rms})/T'_{l,rms}$ for three channel flows at $M_b = 1.5$ with different Re_b.

concentrate on the relation between u'_l and u'_{nl}, as well as that between T'_l and T'_{nl}. This may open up a new research avenue for modelling the momentum and heat transfers in compressible wall-bounded turbulence, with the SLSE introduced in the present study serving as a helpful tool.

Acknowledgements. We are grateful to the owners of the DNS dataset listed in table 1 for kindly sharing their data. C.C. would like to thank Y. Zhao at SJTU for helpful discussions.

Funding. L.F. acknowledges the fund from the National Natural Science Foundation of China (no. 12422210), the fund from the Research Grants Council (RGC) of the Government of Hong Kong Special Administrative Region (HKSAR) with RGC/ECS Project (no. 26200222), RGC/GRF Project (no. 16201023) and RGC/STG Project (no. STG2/E-605/23-N), the fund from Guangdong Basic and Applied Basic Research Foundation (no. 2024A1515011798), the fund from Guangdong Province Science and Technology Plan Project (no. 2023A0505030005), the fund from CORE as a joint research centre for ocean research between Laoshan Laboratory and HKUST, and the fund from the Project of Hetao Shenzhen-Hong Kong Science and Technology Innovation Cooperation Zone (no. HZQB-KCZYB-2020083).

Declaration of interests. The authors report no conflict of interest.

Author ORCID.
Cheng Cheng https://orcid.org/0000-0002-7961-793X;
Lin Fu https://orcid.org/0000-0001-8979-8415.

References

Busemann, A. 1931 *Handbuch der experimentalphysik*, vol. 4. Geest und Portig.

Chen, X., Gan, J. & Fu, L. 2024 An improved Baldwin–Lomax algebraic wall model for high-speed canonical turbulent boundary layers using established scalings. *J. Fluid Mech.* **987**, A7.

Cheng, C., Chen, X., Zhu, W., Shyy, W. & Fu, L. 2024 Progress in physical modeling of compressible wall-bounded turbulent flows. *Acta Mechanica Sin.* **40** (1), 323663.

Cheng, C. & Fu, L. 2022 Large-scale motions and self-similar structures in compressible turbulent channel flows. *Phys. Rev. Fluids* **7** (11), 114604.

Cheng, C. & Fu, L. 2023 Linear-model-based study of the coupling between velocity and temperature fields in compressible turbulent channel flows. *J. Fluid Mech.* **964**, A15.

Cheng, C. & Fu, L. 2024*a* Mean temperature scalings in compressible wall turbulence. *Phys. Rev. Fluids* **9**, 054610.

Cheng, C. & Fu, L. 2024*b* On the streamwise velocity, temperature and passive scalar fields in compressible turbulent channel flows: a viewpoint from multiphysics couplings. *J. Fluid Mech.* **983**, A38.

COGO, M., BAÙ, U., CHINAPPI, M., BERNARDINI, M. & PICANO, F. 2023 Assessment of heat transfer and Mach number effects on high-speed turbulent boundary layers. *J. Fluid Mech.* **974**, A10.

CROCCO, L. 1932 Sulla trasmissione del calore da una lamina piana a un fluido scorrente ad altavelocita. *L Aerotecnica* **12**, 181–197.

VAN DRIEST, E.R. 1951 Turbulent boundary layer in compressible fluids. *J. Aeronaut. Sci.* **18** (3), 145–160.

DUAN, L. & MARTIN, M.P. 2011 Direct numerical simulation of hypersonic turbulent boundary layers. Part 4. Effect of high enthalpy. *J. Fluid Mech.* **684**, 25–59.

FU, L., KARP, M., BOSE, S.T., MOIN, P. & URZAY, J. 2021 Shock-induced heating and transition to turbulence in a hypersonic boundary layer. *J. Fluid Mech.* **909**, A8.

GAVIGLIO, J. 1987 Reynolds analogies and experimental study of heat transfer in the supersonic boundary layer. *Intl J. Heat Mass Transfer* **30** (5), 911–926.

GRIFFIN, K.P., FU, L. & MOIN, P. 2023 Near-wall model for compressible turbulent boundary layers based on an inverse velocity transformation. *J. Fluid Mech.* **970**, A36.

GUARINI, S.E., MOSER, R.D., SHARIFF, K. & WRAY, A. 2000 Direct numerical simulation of a supersonic turbulent boundary layer at Mach 2.5. *J. Fluid Mech.* **414**, 1–33.

HASAN, A.M., LARSSON, J., PIROZZOLI, S. & PECNIK, R. 2024 Estimating mean profiles and fluxes in high-speed turbulent boundary layers using inner/outer-layer scalings. *AIAA J.* **62** (2), 848–853.

HUANG, J., DUAN, L. & CHOUDHARI, M.M. 2022 Direct numerical simulation of hypersonic turbulent boundary layers: effect of spatial evolution and Reynolds number. *J. Fluid Mech.* **937**, A3.

HUANG, P.G., COLEMAN, G.N. & BRADSHAW, P. 1995 Compressible turbulent channel flows: DNS results and modelling. *J. Fluid Mech.* **305**, 185–218.

JIMÉNEZ, J. 2018 Coherent structures in wall-bounded turbulence. *J. Fluid Mech.* **842**, P1.

MODESTI, D. & PIROZZOLI, S. 2016 Reynolds and Mach number effects in compressible turbulent channel flow. *Intl J. Heat Fluid Flow* **59**, 33–49.

MORKOVIN, M.V. 1962 Effects of compressibility on turbulent flows. *Mécanique de la Turbulence* **367** (380), 26.

PIROZZOLI, S., GRASSO, F. & GATSKI, T.B. 2004 Direct numerical simulation and analysis of a spatially evolving supersonic turbulent boundary layer at $M = 2.25$. *Phys. Fluids* **16** (3), 530–545.

SONG, Y., ZHANG, P. & XIA, Z. 2023 Predicting mean profiles in compressible turbulent channel and pipe flows. *Phys. Rev. Fluids* **8** (3), 034604.

WALZ, A. 1962 Compressible turbulent boundary layers, pp. 299–350. CNRS.

ZHANG, C., DUAN, L. & CHOUDHARI, M.M. 2018 Direct numerical simulation database for supersonic and hypersonic turbulent boundary layers. *AIAA J.* **56** (11), 4297–4311.

ZHANG, P.J.Y., WAN, Z.H., LIU, N.S., SUN, D.J. & LU, X.Y. 2022 Wall-cooling effects on pressure fluctuations in compressible turbulent boundary layers from subsonic to hypersonic regimes. *J. Fluid Mech.* **946**, A14.

ZHANG, Y.S., BI, W.T., HUSSAIN, F. & SHE, Z.S. 2014 A generalized Reynolds analogy for compressible wall-bounded turbulent flows. *J. Fluid Mech.* **739**, 392–420.